Seventh International Conference on CFD in the Minerals and Process Industries
CSIRO, Melbourne, Australia
9-11 December 2009

COMPREHENSIVE DEM-DPM-CFD SIMULATIONS - MODEL SYNTHESIS, EXPERIMENTAL VALIDATION AND SCALABILITY

Christoph KLOSS[1], Christoph GONIVA[1], Georg AICHINGER[3] and Stefan PIRKER[1,2]

[1] Christian Doppler Laboratory on Particulate Flow Modelling
[2] Institute of Fluid Mechanics and Heat Transfer
both Johannes Kepler University, Altenbergerstr. 69, 4040 Linz, Austria
[3] Siemens VAI Metals and Technologies, IR DR Technology, Turmstr.44, 4031 Linz, Austria

ABSTRACT

We report on the synthesis of the Discrete Element Method (DEM) modelling the behaviour of granular materials and a finite volume model for the continuous interstitial fluid using Computational Fluid Dynamics (CFD). DEM captures the physics of granular materials best but is computationally time-consuming. For this reason, the DEM is complemented by a Discrete Phase Model (DPM) for disperse granular flow in order to accelerate the overall simulation. In our case, both DEM and DPM are applied within one simulation by using spatial domain decomposition. The implementation of the code permits fully parallel simulations for all three models. We demonstrate the efficiency and validity of our approach by three validation examples and discuss the scalability of the coupling approach.

NOMENCLATURE

C_d	drag coefficient
Cu	Cundall number
Cu^*	modified Cundall number
d	diameter
$\mathbf{f}_p$	force density the particles exert on the fluid
$\mathbf{F}_f$	sum of all forces the fluid exerts on a single particle
$\mathbf{g}$	gravity constant
p	pressure
$\mathbf{u}$	velocity
$\Delta\mathbf{u}_p$	relative particle velocity at contact point
Re_p	particle Reynolds number
$\Delta\mathbf{x}_p$	particle overlap at contact point

Subscript indices:

f	fluid
n	normal to contact point
p	particle
t	tangential to contact point

Greek letters:

α	volume fraction
μ	dynamic viscosity
μ_c	Coulomb friction coefficient
ρ	density
$\boldsymbol{\tau}$	stress tensor
$\boldsymbol{\omega}$	angular velocity

INTRODUCTION

Generally, two modelling strategies for particle flow can be applied. The continuum approach considers the multitude of particles as an artificial continuum and is based on the solution of the underlying conservation equations using CFD techniques. Of course, such an approach disregards the local behaviour of individual particles. The so-called kinetic theory for granular flow has been introduced and successfully applied in many cases, but as it stems from kinetic gas theory, the application is limited to cases where the motion of the particles resembles the motion of molecules in a gas. However, in systems comprising particles that are evenly distributed with the same bulk properties so that they can be thought of as forming a continuum, such an approach can yield results that are in qualitative agreement with experimental data.

The second modelling strategy does not rely upon continuum mechanics. It rather simulates the motion of each particle individually, with a special treatment for eventual collisions. Many such methods have been developed over the years. They can be subdivided into two categories. The first category comprises the probabilistic methods that are based on randomly displacing the particles in the simulation domain, instead of directly resolving interparticle collisions. If the interparticle collisions are important, but not dominant, statistical methods might be used to model their influence (Sommerfeld, 2001; Kahrimanovic et al, 2008; Kloss and Pirker, 2008). The second category of discrete models is the Discrete Element Method and its derivates. Lately, the DEM comes more and more into the focus of engineers and researchers. Being discrete in nature, it is, in principal, capable of capturing all granular physical phenomena. On the other hand, the DEM leads to massive CPU effort making it impossible to simulate large scale industrial processes with a straight-forward approach.

Practically, none of all those granular models has been proven to describe general granular flow situations with reasonable CPU effort.

Furthermore, single phase 'dry' granular flow rarely occurs. In the vast majority of natural or industrial processes concerning granular materials, a secondary fluid phase, such as air, is present and its effects like fluidization (aeration of particles by gas injection) play an important role.

In the following section, we give a brief overview of our modelling approach. We then present and discuss our test cases before drawing final conclusions in the last section.

MODEL DESCRIPTION

Since in many cases different granular regimes occur within one simulation, a synthesis of individually dedicated models is considered to be the best trade-off between capturing the physics and ensuring computability. The actual coupling is implemented by joining the two commercial software packages EDEM and FLUENT by an in-house code. While the former covers the DEM modelling, the latter describes the fluid dynamics of the continuous phase and the motion of particles in dilute flow regimes by means of the Discrete Phase Model.

A further implementation of the coupling, using the open-source software OpenFOAM as CFD solver and the molecular dynamics software LAMMPS (sse plimptom, 1995) as DEM solver, was also developed, and is yet in beta stadium.

From a physical point of view, the coupling currently comprises the effect of (a) volume displacement by the particles, (b) drag of the fluid on the particles as well as (c) Magnus force due to particle rotation.

Discrete Element Method (DEM)

The Discrete Element Method was introduced by Cundall and Strack (1979). In the frame of the DEM, all particles in the computational domain are tracked in a Lagrangian way, explicitly solving each particle's trajectory, based on corresponding momentum balances for translational and angular accelerations. A very brief description of the method will be provided in this section. Further details on the contact physics and implementational issues are available in the literature (e.g. Campbell, 1990; Zhou et al., 1999; Mattutis et al., 2000; Bertrand et al., 2005).

Generally, the particles are allowed to overlap slightly. The normal force tending to repulse the particles can then be deduced from this spatial overlap $\Delta\mathbf{x}_p$ and the normal relative velocity at the contact point, $\Delta\mathbf{u}_n$. The simplest example is a linear spring-dashpot model:

$$\mathbf{F_n} = -k_n \Delta\mathbf{x_p} + c_n \Delta\mathbf{u_{p,n}} \tag{1}$$

The magnitude of the tangential contact force can be written as:

$$\mathbf{F_t} = min\left\{ \left| k_t \int_{t_{c,0}}^{t} \Delta\mathbf{u_{p,t}} dt + c_t \Delta\mathbf{u_{p,t}} \right|, \mu_c \mathbf{F_n} \right\}, \tag{2}$$

where F_t is the tangential force and $\Delta u_{p,t}$ is the relative tangential velocity of the particles in contact. The integral term represents an incremental spring that stores energy from the relative tangential motion, representing the elastic tangential deformation of the particle surfaces. The second part, the dashpot, accounts for the energy dissipation of the tangential contact. The magnitude of the tangential force is limited by the Coulomb frictional limit, where the particles begin to slide over each other. Subsequently, the total force acting on a particle can then be expressed as:

$$\mathbf{F_{tot}} = \mathbf{F_n} + \mathbf{F_t} + \mathbf{F_f} + \mathbf{F_b} \ . \tag{3}$$

Here, $\mathbf{F}_f$ is the force that the fluid phase exerts on the particles, which will be described in further detail later. Other body forces like gravity, electrostatic or magnetic forces are subsumed into $\mathbf{F}_b$.

Similar balances are necessary for the particles' angular momentum which are not stated here or the sake of shortness.

The power of the DEM lies in its ability to resolve the granular medium at the particle scale, thus allowing realistic contact force chains and giving rise to phenomena induced by particle geometry combined with relative particle motion, such as particle segregation by percolation. Thereby, it is able to capture many phenomena, describe dense and dilute particulate regimes, rapid flow as well as slow flow and equilibrium states or wave propagation within the granular material.

The drawback of the method is that the time-step has to be chosen extremely small because the contact force exhibits a very stiff behaviour. Depending on the material properties and the particle size the time-step size can be as low as in the order of 10^{-6} sec for an accurate simulation.

Thanks to advancing computational power, the DEM has become more and more accessible lately. On actual desktop computers, simulations of up to a million particles can be performed. On very large clusters, the trajectories of hundreds of millions of particles can be computed.

CFD Approach

The motion of the fluid phase in the presence of a secondary particulate phase is governed by a modified set of Navier-Stokes-Equations, which can be written as:

$$\frac{\partial \alpha_f}{\partial t} + \nabla \cdot \left(\alpha_f \, \mathbf{u_f} \right) = 0, \tag{4}$$

$$\frac{\partial \left(\rho_f \, \alpha_f \, \mathbf{u_f} \right)}{\partial t} + \nabla \cdot \left(\rho_f \, \alpha_f \, \mathbf{u_f} \, \mathbf{u_f} \right) = -\nabla p - \mathbf{f_p} + \nabla \cdot \left(\alpha_f \ \boldsymbol{\tau} \right) + \rho_f \, \alpha_f \ \mathbf{g}. \tag{5}$$

Here, α_f is the volume fraction occupied by the fluid, ρ_f is its density, $\mathbf{u}_f$ its velocity, $\boldsymbol{\tau}$ is the stress tensor for the fluid phase and $\mathbf{f}_p$ represents the momentum exchange with the particulate phase. For each cell, it is calculated from the forces $\mathbf{F}_f$ (described in the following section) for all particles residing within this cell. If $\mathbf{F}_f$ comprises only drag force, this term is also called generalized drag.

DEM-CFD interaction

To implement the coupling, the DEM solver EDEM and the CFD solver FLUENT are being run either consecutively or concurrently, each halting calculation after a predefined number of time-steps for the purpose of data exchange managed by our software. This data exchange routine consists of several steps:

- For each particle, the corresponding cell in the CFD grid is determined.
- The volume fraction occupied by the granular phase is calculated.
- Based on this information, the momentum exchange terms between the gas phase and the particulate phase can be evaluated.

The most important contribution to particle-fluid momentum exchange is established by means of a drag force depending on the particle volume fraction. Certain empirical or semi-empirical approaches have been published to model this force. In our coupling software

package, we use a model by Gidaspow (1994) combining models for the dilute and dense granular regime. This model is very common, but the transition between the dilute regime and the dense regime is discontinuous, which could lead to convergence problems. Therefore, in addition to Gidaspow's model, we alternatively make use of a drag model by Di Felice, also used by Yu et al. (2008):

$$\mathbf{F_d} = \frac{1}{2}\rho_f \left(\mathbf{u_f} - \mathbf{u_p}\right)\left|\mathbf{u_f} - \mathbf{u_p}\right| C_d \frac{{d_p}^2 \pi}{4} {\alpha_f}^{1-\chi}. \qquad (6)$$

$$C_d = \left(0.63 + \frac{4.8}{\mathrm{Re}_p}\right)^2, \qquad (7)$$

$$\chi = 3.7 - 0.65 exp\left[-\frac{\left(1.5 - log_{10}\mathrm{Re}_p\right)^2}{2}\right], \qquad (8)$$

$$\mathrm{Re}_p = \frac{\rho_f d_p \alpha_f \left|\mathbf{u_f} - \mathbf{u_p}\right|}{\mu_f}. \qquad (9)$$

Further literature on similar approaches can be found in Yu et al. (2008), Tsuji et al. (2008) and Kafui et al. (2002). Beside the drag force resulting from a relative velocity between the particle and the fluid, other forces may be relevant too. These may stem from the pressure gradient in the flow field (pressure force), from particle rotation (Magnus force), particle acceleration (virtual mass force) or a fluid velocity gradient leading to shear (Saffman force). The force $\mathbf{F}_f$ exerted by the fluid phase on a single particle is then the sum of all these forces.

For the pneumatic conveying example, drag force and Magnus force are being accounted for, $\mathbf{F}_f = \mathbf{F}_d + \mathbf{F}_m$. The Magnus force formulation used is given by Lun et al. (1997). For the other validation examples, all other forces than the drag force can be neglected, so that $\mathbf{F}_f = \mathbf{F}_d$.

Discrete Phase Model (DPM)

The standard Lagrangian DPM is, like the DEM, based on a translational force balance that is formulated for an individual particle.

In the standard DPM, each particle represents a parcel of particles. Like DEM particles, a DPM parcel is subject to gravity, drag force, pressure force, Magnus force, virtual mass force and Saffman force, not all of which are available in the commercial package FLUENT.

A crucial difference to DEM is that in the frame of DPM, interparticle collisions are neglected. Since the DPM also neglects the gas displacement by the particles, the volume fraction of the gas phase remains constant.

Due to this assumptions and simplifications, the DPM is valid for dilute fluid-particle flow only. Recommendations for the applicability vary in literature. In our validation case III, the DPM is applied for parts of the domain where the particle volume fraction is below 5%. The advantage over the DEM is however, that time-steps in the order of 10^{-4} sec can be used.

DEM-DPM interaction

Fully coupled DEM-CFD simulations require a lot of computational effort in terms of CPU performance and memory requirement. If interparticle collisions can be neglected, it is permissible to use the DPM to account for the particulate phase's motion. The actual coupling is realised by static domain decomposition. If a particle's trajectory traverses the predetermined boundary between the DEM and the DPM domain, the particle is transferred from one program to the other. For future applications, it is desired to automatically switch between DEM and DPM depending on the local particle volume fraction. In our implementation, a DPM parcel represents only one particle. Therefore, it is possible to transfer particles from DPM to DEM without loss of information.

The interaction with the fluid phase is calculated as described in the section "DEM-CFD interaction" for all particles, irrespective of whether the particle motion itself is handled by DEM or DPM.

VALIDATION EXAMPLES

In this section, the models described are applied to three cases:

- First, particle rope formation and dispersion during pneumatic conveying is focused (case I).
- Next, particle discharge from a hopper-standpipe configuration is addressed (case II).
- Finally, we discuss the charging of particles into a test facility (case III).

The first two cases are examined using coupled DEM-CFD simulations. In the third case, all three models (DEM, DPM, and CFD) are used within one simulation

For all of the cases, spherical beads made of soda lime glass are used. The wall materials are glass and sheet metal for case I, and Perspex for case II and III.

Case I: Pneumatic Conveying

The pneumatic conveying facility consists of a radial fan followed by a particle injector fed by a vibrator chute. A double–looping is placed right after the injector, providing for the formation of a particle strand caused by centrifugal forces. The double-looping is followed by the measurement section. The geometry of the measuring channel is shown in Fig. 1. At these positions, measurements using a Particle Image Velocimetry (PIV) system can be conducted. The volume concentration can be evaluated as well by digital image processing. This technique has been published in detail by Kloss and Pirker (2008). For further details on the design of the pneumatic conveying facility itself, the reader is referred to Kahrimanovic et al. (2008). Because air density is much lower than particle density, forces like the Basset force or virtual mass force can be neglected. Furthermore, the Saffman force is negligible too. On the other hand, the Magnus force is found to have an important effect on the particle volume fraction profile. To study this effect, the simulation was conducted with and without the Magnus force.

The simulation is carried out with an air mass-flow of 0.18 kg/s and a granular mass-flow (particle diameter 0.85 mm) of 0.09 kg/s, corresponding to a mass loading of 0.5. The total number of particles in the simulation is around 200,000. Simular simulations with higher mass loadings have been performed with up to 600,000 particles though. The CFD grid contained around 100,000 cells.

The dedicated velocity and volume fraction profiles for position 3 are shown in Fig. 2. "Left", "Middle" and "Right" refer to the left, center and right sections of the profile as marked in Fig. 1.

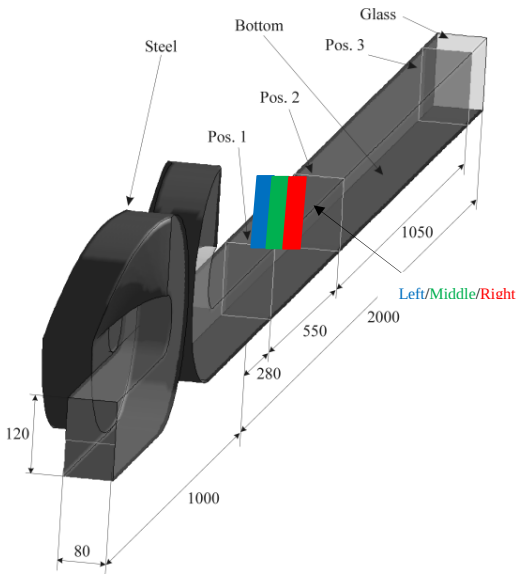

Figure 1: Geometry of the double-looping and the measurement channel, taken from Kahrimanovic et al. (2008). All values are in mm.

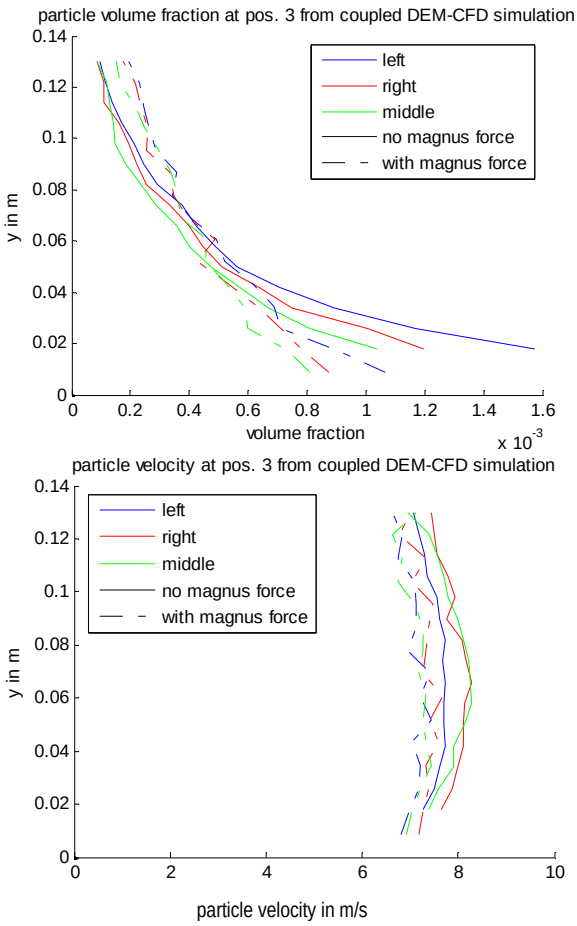

Figure 2: Profiles of volume fraction and particle velocity for position 3 from coupled DEM-CFD simulation,where y is the height over the channel ground.

One can deduce from Fig. 2 that the Magnus force, stemming from particle rotation induced by collisions, especially in the double-looping, tends to dissolve the particle strand and to even out the volume fraction profile while slightly decreasing the particle velocity. Generally, the particle volume fraction lowers as the particles are accelerated by the gas phase. As the Magnus force tends to dissolve the particle strand, the solids fraction profiles at positions 2 and 3 (not shown) are steeper than at position 1.

In Fig. 3, comparisons of measured and simulated profiles for position 3 are given. At position 3, the agreement of the volume fraction profiles is quite good. At positions 1 and 2, the experimental and numerical profiles do show deviations. This could be due to the fact that wall roughness has not been accounted for in the simulation. Kahrimanovic et al. (2008) found out that the influence of wall roughness may be of high importance when it comes to particle strand dispersion at a wall.

Case II: Hopper Discharge

The second example is the discharge of glass beads (4 mm in diameter) from a hopper with enclosed standpipe. The hopper is made of Perspex and exhibits a hopper angle of 10°. It can thus be regarded as a mass-flow hopper. The geometry and a simulation snapshot are shown in Fig. 4. The evolving granular mass-flow in the simulation is 0.097 kg/s.

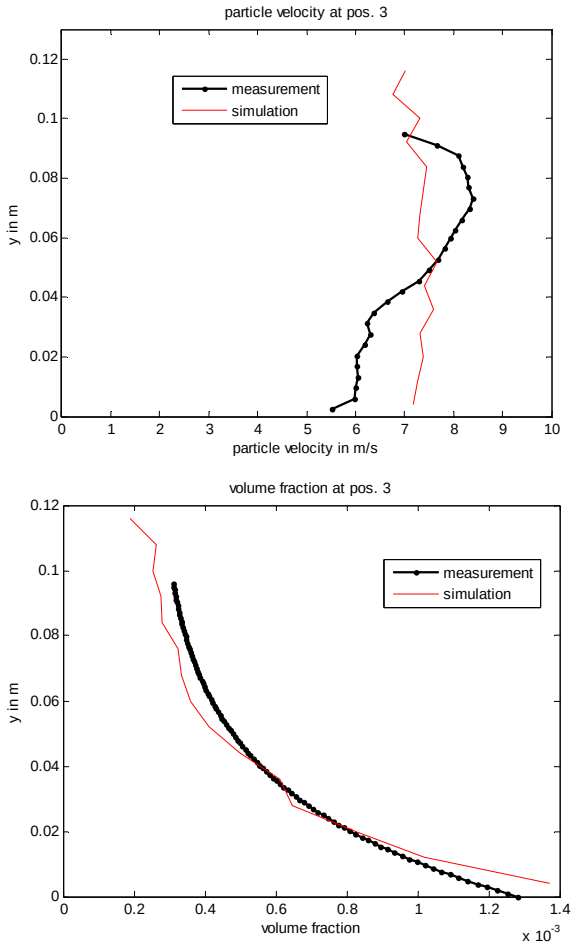

Figure 3: Comparison of the profiles of volume fraction and particle velocity from measurement and from simulation at position 3, where y is the height over the channel ground.

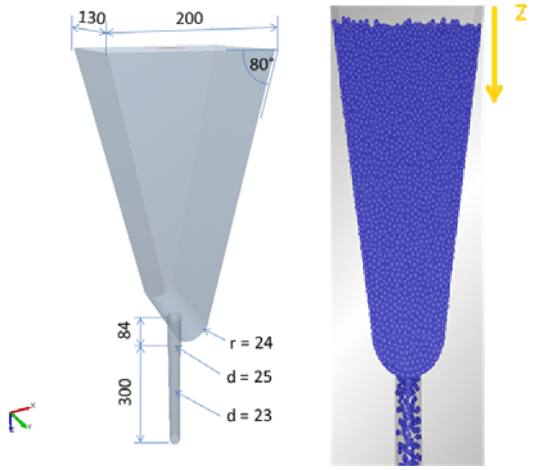

Figure 4: Geometry of the hopper-standpipe combination (left, all values in mm) and simulation snapshot during discharge (right).

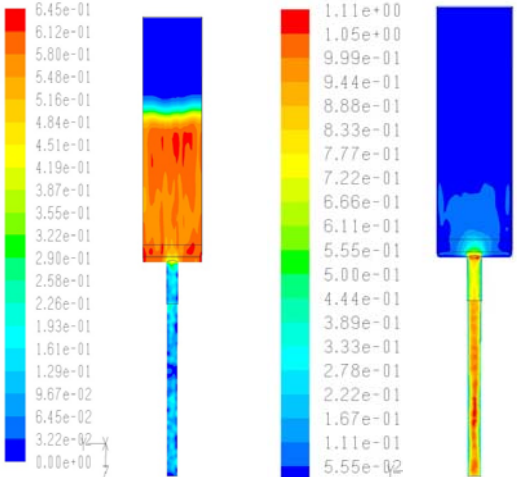

Figure 5: Snapshot of the solids fraction in the y-z plane during discharge (left) and flow field of the fluid phase in the symmetry plane during discharge in m/s (right).

The CFD grid size and number of particles are 25,000 and 60,000, respectively. A snapshot of the particle volume fraction during discharge is shown on the left hand side of Fig. 5.

It is well reported in literature (e.g. Rao and Nott, 2008) that the addition of a standpipe to a hopper may increase the discharge flow rate. This is because the particles flowing out of the hopper accelerate the air phase that surrounds them. In the absence of the standpipe, this would lead to a flow of surrounding air towards the falling particle strand in order to fulfil the mass-balance for the gas phase. In the presence of the standpipe, suction from the side is not possible, so the air is forced to come from the hopper, accelerating the particles close to the orifice and thus resulting in a higher discharge rate. In the area around the orifice, the particles are accelerated by the fluid, whereas in the lower section of the standpipe, momentum is transferred in the other direction - from the particles to the fluid.

However, this effect is only dominant for small particle sizes (well below 1 mm). In our case, this effect has no significant influence on the particle flow rate, and we can regard the flow as induced by the particle motion

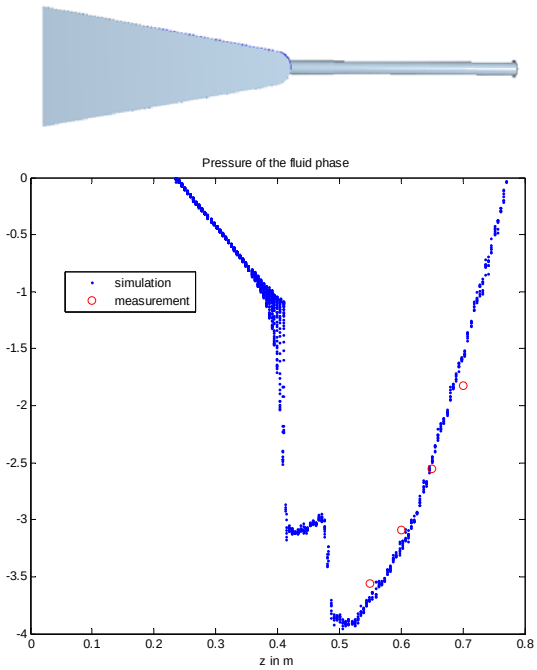

Figure 6: Pressure of the fluid phase over z together with the geometry of the hopper.

with hardly any feedback influence on the particles (one-way-coupling in a physical point of view).

The pressure of the fluid phase is shown in Fig. 6. Each distinct point in the figure is the pressure in one computational cell. The drop at z=0.4 is caused by the transition from the hopper to the standpipe. The higher values correspond to cells at the edge of the hopper, where the air is de facto at rest, whereas the lower values are reached in cells close to the standpipe. The pressure change at z=0.47 m is caused by a change in the standpipe's cross-sectional area.

At the end of the standpipe (corresponding to z=0.77 m), ambient pressure is reached again. The pressure values inside the standpipe have been measured with dedicated sensors. The good agreement with the pressure from the simulation indicates that the flow field within the standpipe is well reproduced by the simulation.

Case III: Particle Charging

In our third example, we report on the segregation of a bi-disperse mixture of glass spheres inside a laboratory-scale experiment. This is inspired by metallurgical charging processes, where industry has the need of better understanding and optimizing charging and the bed build-up processes.

The diameter distribution consists of two spherical fractions:

- 30 mass-% of diameter 1.125 mm, and
- 70 mass-% of diameter 3.075 mm.

The facility is made of Perspex and consists of an initial free-fall section, a steep (60°) chute flow and a further free fall-section. The granular mass-flow is chosen to be 150 g/s. The particles are released from a hopper identical to the one shown in Fig. 4 (without the standpipe) into free fall. The particles inside the hoppers are assumed to be ideally mixed. Details on the geometry are depicted in Fig. 7. The depth of the set-up is 5 cm.

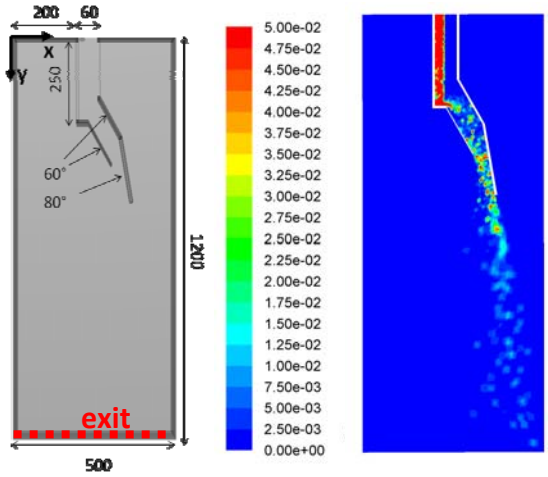

Figure 7: Geometry of the charging experiment (left; lengths in mm, angles are relative to horizontal) and particle volume fraction in the symmetry plane, capped at 5% (right).

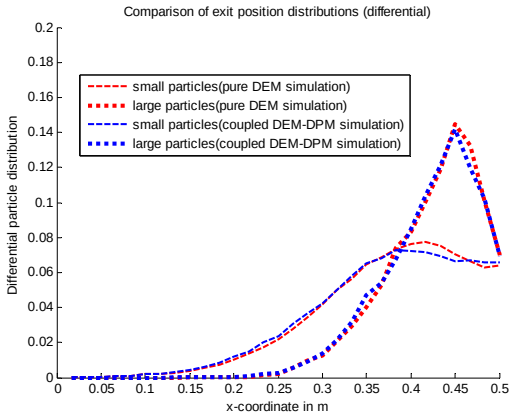

Figure 8: Comparison of DEM and DPM results for the exit x-position distribution for both particle fractions.

In the simulation, the particles are removed from the computational area as soon as they exceed y>1.2 m (the red line as depicted in Fig.7). Fig. 7 also shows the local particle volume fraction in the symmetry plane of the geometry.

The domain decomposition is shown in Fig. 9. DEM is used where the volume fraction locally exceeds 5%. To validate that the use of DPM is justified in this case, the DPM result for the particles' exit distributions for x-position and velocity magnitude are compared with a simulation where the particles' motion is completely handled by DEM. As one can see from Fig. 8 and 10, the results are nearly perfectly identical.

PERFORMANCE AND SCALABILITY

Scaling of the Parallel DEM-CFD Coupling

With our in-house code, truly parallel computation of coupled DEM, DPM and CFD simulations are possible (which is not possible within the commercially available coupling module). As de facto all of the CPU consuming operations needed to perform the DEM-CFD coupling are executed within the CFD code, it is assured that the parallel scaling of the DEM part is not impaired by the coupling. The scaling of the CFD code is shown in Fig. 11.

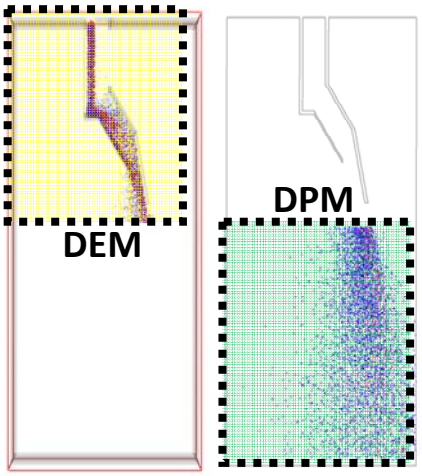

Figure 9: Domain decomposition: The upper part of the computational domain the particles' motion is handled by DEM, the lower part it is handled by DPM. The particles are coloured by size (red=large, blue=small).

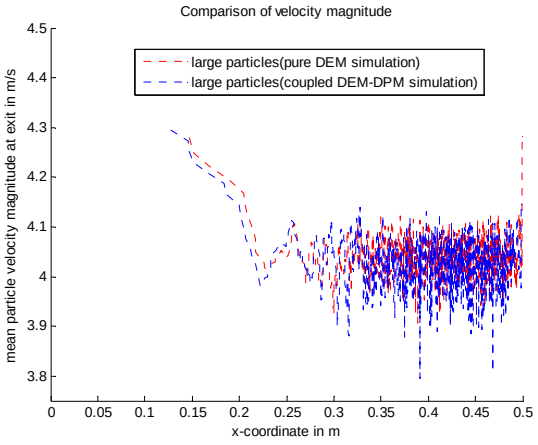

Figure 10: Comparison of DEM and DPM results for the exit velocity distribution for the large particle fraction.

DEM-DPM Speed Up

To compare the efficiency of different DEM algorithms, the so-called Cundall number *Cu* is often used. It is defined as the number of particle time-steps per CPU second. *Cu* is independent of the machine, but depends on the coordination number. To compare the computational efficiency of DEM and DPM, we must use a quantity that accounts for the different time-step sizes of the two algorithms. For our case, one might use a modified Cundall number calculated from the real time simulated, the total number of particles in the domain, the time the algorithm takes to run, and the number of CPUs that were used:

$$Cu^* = \frac{t_{real} N_p}{t_{run} N_{CPU}}. \qquad (10)$$

Although this number depends on the machine that the simulation is run on, the ratio Cu^*_{DPM}/Cu^*_{DEM} should be independent of the machine the simulation is running on. In our case, although the DPM load balance was not optimized, a considerable speed-up of $Cu^*_{DPM}/Cu^*_{DEM} = 4$ could be reached. Thus, the particles within the DPM domain are calculated four times faster than their counterparts in the DEM domain.

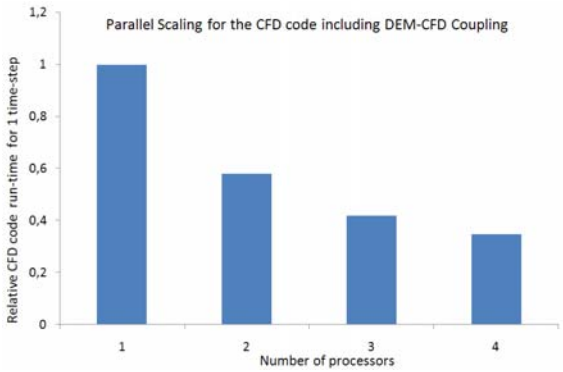

Figure 11: Parallel scaling of the CFD code including DEM-CFD coupling. The measurements were performed for case I (pneumatic conveying).

CONCLUSION

Coupled DEM-CFD simulations can govern a huge variety of regimes. We showed one example with high solids fraction (the hopper discharge) and one example with low solids fraction (the pneumatic conveying). While in the case of our hopper discharge example the fluid flow can be regarded as to be induced by particle motion with hardly any feedback to the particles, in the case of pneumatic conveying the particle motion is controlled by the gas flow.

As the DEM is very CPU intense, it is useful to complement it by further models for particle flow that are less CPU expensive. We showed that in the case of the particle charging experiment, the simulation can be significantly sped up by switching from DEM to DPM in dilute regions where the effect of interparticle collision can be neglected without any significant effects on the result. Thus, we can conclude that the synthesis of DEM, DPM and the CFD method leads to a very versatile tool with many possibilities of application.

ACKNOWLEDGEMENTS

This study was partly funded by the Christian Doppler Gesellschaft (www.cdg.at) of the Austrian government.

REFERENCES

BERTRAND, F., LECLAIRE, L.-A. and LEVECQUE, G. (2005): "DEM-based models for the mixing of granular materials", *Chemical Engineering Science*, **60**, 2517 – 2531

CAMPBELL, C. S. (1990): "Rapid Granular Flows", *Annual Rev. Fluid Mech.*, **22**, 57-92.

CUNDALL, P.A. and STRACK, O.D. (1979): "A discrete numerical model for granular assemblies." *Geotechnique*, **21**, 47-65

GIDASPOW, D. (1994): "Multiphase Flow and Fluidization", *Academic Press*, Boston.

KAFUI, K.D., THORNTON, C., ADAMS, M. J. (2002): "Discrete particle-continuum modelling of gas–solid fluidised beds", *Chemical Engineering Science*, **57**, 2395 – 2410

KAHRIMANOVIC, D., KLOSS, C. and PIRKER, S. (2008): "Numerical Study and Experimantal Validation of Particle Strand Formation", *Proceedings of the 6th International Conference on CFD in Oil & Gas, Metallurgical and Process Industries*, SINTEF/NTNU, Trondheim, Norway, June 10-12

KLOSS, C. and PIRKER, S. (2008): "Implementation and Experimental Validation of a Stochastical Interparticle Collision Model", *Proceedings of the 6th International Conference on CFD in Oil & Gas, Metallurgical and Process Industries*, SINTEF/NTNU, Trondheim, Norway, June 10-12

LUN, C.K.K. and LIU H.S. (1997): "Numerical simulation of dilute turbulent gas-solid flows in horizontal channels", *Int. J. Multiphase Flow*, **23**, 575-605

MATUTTIS, H.G., LUDING S. and HERRMANN, H.J. (2000): "Discrete element simulations of dense packings and heaps made of spherical and non-spherical particles", *Powder Technology*, **109**, 278–292

PLIMPTON, S. J. (1995), "Fast Parallel Algorithms for Short-Range Molecular Dynamics", *J. Comp. Phys.*, **117**, 1-19 (LAMMPS homepage: http://lammps.sandia.gov).

RAO, K.K. and NOTT, P.R. (2008): "An Introduction to Granular Flow", *Cambridge Series in Chemical Engineering*, Cambridge

SOMMERFELD, M. (2001): "Validation of a stochastic Lagrangian modelling approach for inter-particle collisions in homogeneous isotropic turbulence", *Int. J. Multiphase Flow*, **27**, 1829 – 1858.

TSUJI, T., YABUMOTO, K. and TANAKA, T. (2008): "Spontaneous structures in three-dimensional bubbling gas-fluidized bed by parallel DEM–CFD coupling simulation", *Powder Technology*, **184**, 132–140

YU, A.B., WRIGHT, B., ZHOU, Z.Y, ZHU, H.P., and ZULLI, P. (2008): "Discrete particle simulation of gas-solids flow in a blast-furnace", *Computers & Chemical Engineering*, **32**, 1760-1772

ZHOU, Y.C., WRIGHT, B.D., YANG, R.Y., XU, B.H., YU, A.B. (1999): "Rolling friction in the dynamic simulation of sandpile formation", *Physica A*, **269**, 536-553

